Journal of Power Sources 195 (2010) 6688–6698

Contents lists available at ScienceDirect

Journal of Power Sources

journal homepage: www.elsevier.com/locate/jpowsour

Radiative and convective heat transport within tubular solid-oxide fuel-cell stacks

Robert J. Kee [a,*], Benjamin L. Kee [a], Jerry L. Martin [b]

[a] Engineering Division, Colorado School of Mines, 1600 Illinois St., Golden, CO 80401, USA
[b] DellaTech, LLC, Superior, CO 80027, USA

ARTICLE INFO

Article history:
Received 6 February 2010
Received in revised form 5 April 2010
Accepted 5 April 2010
Available online 13 April 2010

Keywords:
Tubular SOFC
Long cylinder bundle
Thermal radiation
Configuration factors

ABSTRACT

This paper develops a relatively simple model that is intended to rapidly evaluate design configuration and operating conditions for tubular anode-supported solid-oxide fuel-cell (SOFC) stacks. Heat is removed from the SOFC tubes by a combination of convection and radiation. Heat is convected to air that circulates outside the SOFC tubes and radiated to a surrounding cylindrical wall. The tubes are assumed to be arranged in hexagonal arrays in which the distance between tubes centers form equilateral triangles. The paper presents new configuration-factor formulas that are needed to represent arrays of staggered cylinders. The configuration factors are derived for long cylinders using the crossed-string method. These configuration factors have general utility beyond the application to fuel-cell systems. The model is applied to a particular cell and stack system and used to evaluate the effects of a range of design and operating conditions.

1. Introduction

Fig. 1 illustrates a fuel-cell bundle comprised of three hexagonal tube "rings." The center cylinder is a structural support, which may have gases flowing through it. In practice, the stack is surrounded by an outer cylindrical shell and thermal insulation. The fuel cells are typically an anode-supported architecture, with fuel flowing inside the tubes and air flowing outside [1,2]. Tubular stacks are usually connected in series, with each cell producing nominally the same current and the stack voltage being the sum of the cell voltages. In addition to electricity, the fuel cells produce heat, which must be transferred to the environment. The heat is carried out by convection to surrounding cathode air and by radiation to the surrounding shell. Maintaining SOFC temperature and limiting temperature differences between tubes are important considerations in stack design and operating conditions.

Evaluation of the radiation heat transfer within the tube bundle depends upon geometric configuration factors (the configuration factor between two surfaces is defined as the fraction of radiation leaving one surface that is intercepted by the other surface [3]). For a three-dimensional assembly as complex as the one illustrated, the configuration factors must be evaluated computationally. However, if the tubes are sufficiently long, then a two-dimensional approximation is reasonable. In this case, the configuration factors can be evaluated analytically. The model reported here uses the crossed-string method to evaluate the needed configuration factors [3,4].

Juul [5] reports a careful analysis of the differences between full three-dimensional configuration factors for finite-length parallel cylinders and configuration factors evaluated using the crossed-string method. The results are presented in terms of the ratio of the tube separation distance and the tube radii (i.e., s/r) and the ratio of tube length and tube radius (i.e., L/r). For SOFC bundles such as those considered here, s/r is on the order of unity and L/r is on the order of ten or more. Under these circumstances, the two-dimensional crossed-string approach introduces only a 5–10% error, which is consistent with other approximations in the model.

With configuration factors between individual cylinders in hand, a configuration-factor matrix can be evaluated to determine the interactions among all the cylinders in the bundle. By solving a radiosity balance for each cylinder, the net radiation transfer and the cylinder temperatures can be determined. The radiation model is augmented by a convection model that transfers heat between tube surfaces and surrounding air flow. The present model assumes spatially uniform air temperature and a uniform heat-transfer coefficient. The air temperature is determined from an energy balance that depends upon the air mass flow rate. The results show that because the outer tubes serve as de-facto radiation shields, the inner tubes (i.e., those closer to the center post in Fig. 1) generally operate at higher temperature.

There are potentially numerous applications that depend upon heated cylinders being arranged in staggered arrays. Thus, the new

* Corresponding author. Tel.: +1 303 273 3379; fax: +1 303 273 3602.
E-mail address: rjkee@mines.edu (R.J. Kee).

0378-7753/$ – see front matter © 2010 Elsevier B.V. All rights reserved.
doi:10.1016/j.jpowsour.2010.04.010

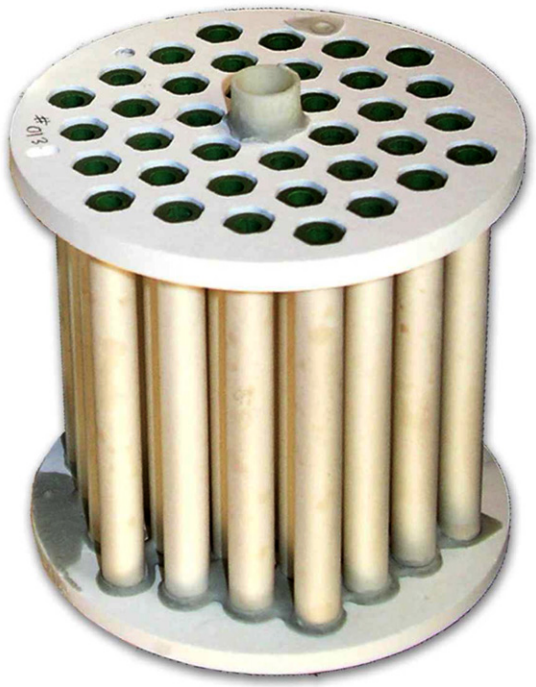

Fig. 1. Photograph of a tubular SOFC stack consisting of three hexagonal rings.

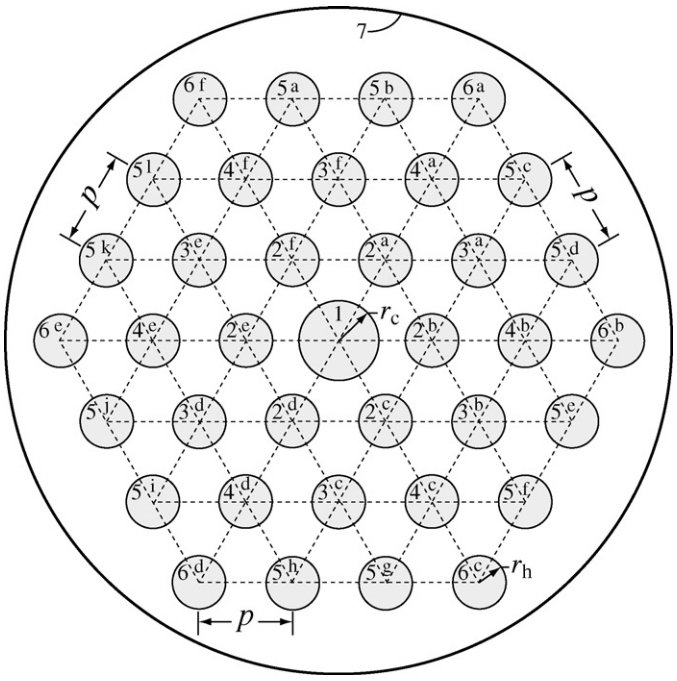

Fig. 2. Hexagonal pattern and numbering of the cylinders.

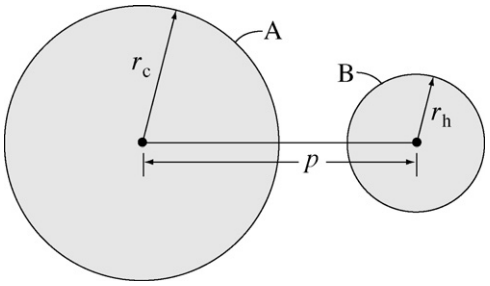

Fig. 3. Geometric layout for the unobstructed configuration factor between parallel cylinders of different radius.

configuration factors that are presented in the paper have general utility.

Although the model presented here is zero-dimensional in the convective heat transfer, it fully captures the overall heat balance. Once the simple model is used to estimate the impact of cathode flow rates, insulation conductance and component emissivities, more detailed models can be used to optimize a design. For example, actual stacks may use cross flow, axial flow or radial flow on the cathode side, or complex flows that are a combination of all three. In these cases, the sensible heat rise in the gas may either enhance or suppress the temperature gradients in the stack. For example, if the cathode air flows radially outward through the tube bundle, the relatively cold air in the center of the bundle will reduce the temperature of the inner tube rows, leading to a reduced gradient across the tube bundle. In the limit of high cathode air flow, or low cathode air inlet temperatures, the radial temperature gradient can even be inverted, with the inner rows of tubes operating at lower temperatures than the outer rows. Similarly, axial air flows can compensate for axial gradients in tube power density.

2. Configuration factors

Fig. 2 illustrates a general layout for which configuration factors are needed. All the cylinders are positioned in a hexagonal pattern. The centers of all cylinders form equilateral triangles with a pitch p. With the exception of the center cylinder, which may be different, all cylinders have radius r_h. The center cylinder has radius r_c. The outer shell has radius r_o. The numbering of the cylinders, which follows that developed by Cox [6,3], facilitates further analysis using the configuration factors. Owing to symmetry, cylinders with the same number behave exactly alike. The example shown in Fig. 2 has six types of cylinders plus the outer shell. The letters are added to assist distinguishing between cylinders in forming composite configuration factors.

The following subsections report configuration factors as functions of the pitch p, radius of the center cylinder r_c, and radius of the cylinders on the hexagonal pattern r_h. Although the algebra can be tedious in some cases, the crossed-string method leads to explicit algebraic formulas. Deriving the configuration factors begins with geometric constructions and trigonometric equations to represent the lengths of the strings. Then MATHEMATICA is used here to simplify symbolically the crossed-string lengths into explicit algebraic expressions [7].

2.1. Unobstructed center to hexagonal parallel cylinders

Fig. 3 illustrates the layout for the unobstructed configuration factor between parallel cylinders of different radius. For example, this situation occurs between the center cylinder 1 and any of the surrounding hexagonal cylinders 2 in Fig. 2. Although this configuration factor is found in most heat-transfer textbooks, it is restated here to incorporate a consistent nomenclature involving p, r_h, and r_c. The configuration factor is:

$$F_{AB} = \frac{r_h}{2r_c} + \frac{1}{2\pi r_c}\sqrt{p^2-(r_c+r_h)^2} - \frac{1}{2\pi r_c}\sqrt{p^2-(r_c-r_h)^2} + \frac{r_c-r_h}{2\pi r_c}\cos^{-1}\left(\frac{r_c-r_h}{p}\right) - \frac{r_c+r_h}{2\pi r_c}\cos^{-1}\left(\frac{r_c+r_h}{p}\right) \quad (1)$$

The only restriction on this configuration factor is that $r_c + r_h \le p$. That is, the cylinders to not overlap.

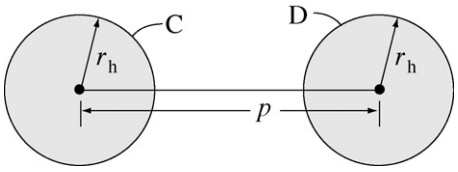

Fig. 4. Geometric layout for the unobstructed configuration factor between parallel cylinders of equal radius.

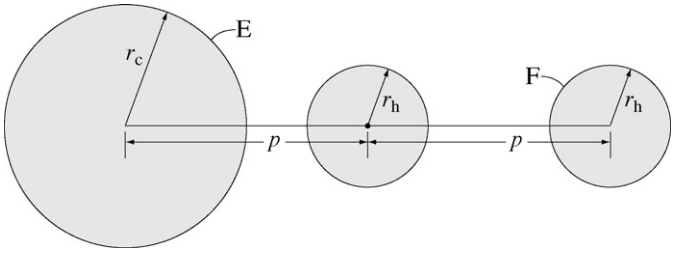

Fig. 5. Geometric layout for the configuration factor between a center cylinder and a hexagonal cylinder, blocked by a co-linear hexagonal cylinder.

2.2. Unobstructed hexagonal to hexagonal cylinders of equal radius

Fig. 4 illustrates the layout for the unobstructed configuration factor between parallel cylinders of equal radius. This configuration factor is clearly a subset of Fig. 3 and Eq. (1). It is only restated here because it is a simpler expression that is used frequently. For example in Fig. 2, this configuration factor applies for 2b to 3b, 2b to 4b, etc.

$$F_{CD} = \frac{1}{2} + \frac{1}{2\pi r_h}\sqrt{p^2 - (2r_h)^2} - \frac{p}{2\pi r_h} - \frac{1}{\pi}\cos^{-1}\left(\frac{2r_h}{p}\right) \tag{2}$$

To assure that the cylinders to not overlap $2r_h \le p$.

2.3. Center to hexagonal cylinder, blocked by a parallel hexagonal cylinder

Fig. 5 illustrates the layout for the configuration factor from a center cylinder (r_c) to a smaller hexagonal cylinder (r_h) that is partially blocked by another hexagonal cylinder (r_h). The centers of the cylinders are co-linear and are separated by the pitch p. For example, in Fig. 2 this situation occurs from 1 to 4b, 1 to 4f, etc. The configuration factor is:

$$F_{EF} = \frac{1}{2\pi r_c}\left[p - \sqrt{4p^2 - (r_c - r_h)^2} + \sqrt{p^2 - (r_c - r_h)^2}\right] + \frac{r_c - r_h}{2\pi r_c}\left[\cos^{-1}\left(\frac{r_c - r_h}{2p}\right) - \cos^{-1}\left(\frac{r_c - r_h}{p}\right)\right] \tag{3}$$

The restrictions on this configuration factor are: $r_c > r_h$ and $r_c + r_h \le p$.

2.4. Center cylinder to hexagonal cylinder, blocked by two co-linear hexagonal cylinders

Fig. 6 illustrates the layout for the configuration factor from a large center cylinder (r_c) to a smaller hexagonal cylinder (r_h) that is blocked by two hexagonal cylinders (r_h). The centers of the cylinders are co-linear and are separated by the pitch p. For example, in Fig. 2 this situation occurs from 1 to 6b, 1 to 6c, etc. The configuration factor is:

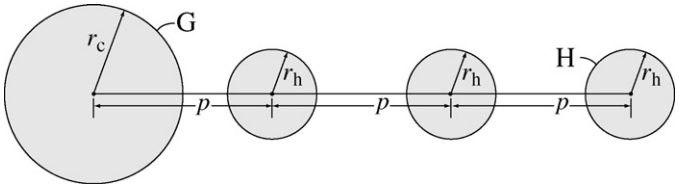

Fig. 6. Geometric layout for the configuration factor between a large center cylinder and a smaller hexagonal cylinder, partially blocked by two smaller co-linear hexagonal cylinders.

$$F_{GH} = \frac{1}{2\pi r_c}\left[p + \sqrt{4p^2 - (r_c - r_h)^2} - \sqrt{9p^2 - (r_c - r_h)^2}\right] + \frac{r_c - r_h}{2\pi r_c}\left[\cos^{-1}\left(\frac{r_c - r_h}{3p}\right) - \cos^{-1}\left(\frac{r_c - r_h}{2p}\right)\right] \tag{4}$$

The restrictions on this configuration factor are: $r_c > r_h$ and $r_c + r_h \le p$. Clearly if $r_c \le r_h$ then no radiation from the center cylinder can reach the far hexagonal cylinder.

2.5. Center cylinder to hexagonal cylinder, blocked by two hexagonal off-axis cylinders

Fig. 7 illustrates the layout for the configuration factor from a center cylinder (r_c) to a hexagonal cylinder (r_h) that is partially blocked by two off-axis hexagonal cylinders (r_h). The centers of all cylinders are located on equilateral triangles having sides of length p. For example, in Fig. 2 this situation occurs from 1 to 3a, 1 to 3b, etc. The configuration factor is:

$$F_{IJ} = \frac{1}{6\pi r_c}[-\pi r_c - 3\pi r_h] + \frac{1}{2\pi r_c}\left[-p\sqrt{1 - \frac{4r_h^2}{p^2}} + \sqrt{3p^2 - (r_c + r_h)^2}\right] + \frac{1}{2\pi r_c}\left[-p\sqrt{1 - \frac{(r_c + r_h)^2}{p^2}}\right] + \frac{1}{2\pi r_c}\left[2r_h\cos^{-1}\left(\frac{2r_h}{p}\right)\right] + \frac{1}{2\pi r_c}\left[(r_c + r_h)\cos^{-1}\left(\frac{r_c + r_h}{p}\right)\right] + \frac{1}{2\pi r_c}\left[(r_c + r_h)\sin^{-1}\left(\frac{r_c + r_h}{\sqrt{3}p}\right)\right] \tag{5}$$

In addition to being restricted by $2r_h \le p$ and $r_c + r_h \le p$, this formula must also satisfy

$$\frac{r_c}{p} \ge \cos\left[\frac{2\pi}{3} - \cos^{-1}\left(2\frac{r_h}{p}\right)\right] - \frac{r_h}{p}. \tag{6}$$

The last restriction prevents the situation that the off-axis do not block the radiation between cylinder 1 and 2. In this case, the configuration factor can be evaluated from Eq. (1), using the separation distance as $\sqrt{3}p$ instead of p.

2.6. Hexagonal cylinder to hexagonal cylinder, blocked by two off-axis hexagonal cylinders

Fig. 8 illustrates the layout for the configuration factor from a hexagonal cylinder (r_h) to another hexagonal cylinder (r_h) that is partially blocked by two off-axis hexagonal cylinders (r_h). The centers of all cylinders are at the apexes of equilateral triangles with sides of length p. This situation is a subset of Fig. 7 and Eq. (5). However, because the situation occurs frequently and the equation is simpler, it is useful to restate the reduced case. For example in

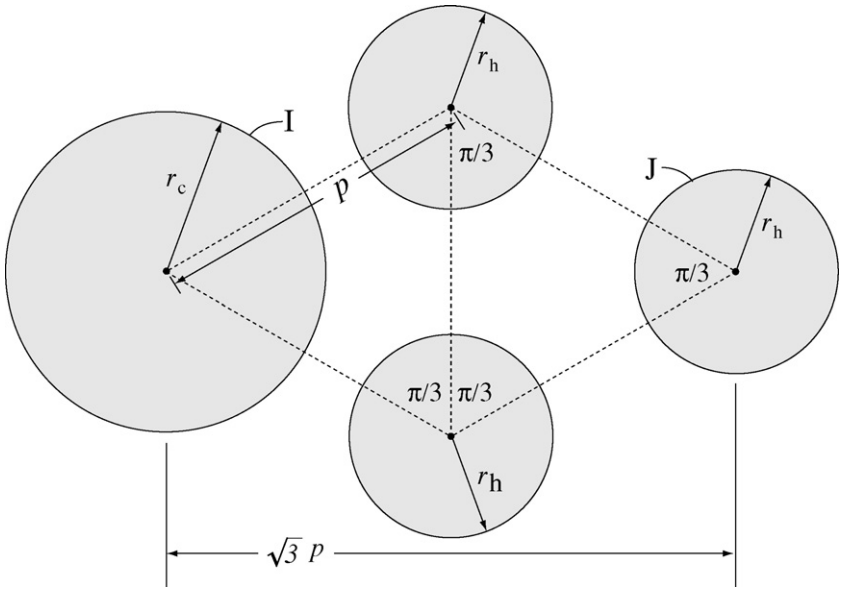

Fig. 7. Geometric layout for the configuration factor between a center cylinder and a hexagonal cylinder, blocked by two off-axis hexagonal cylinders.

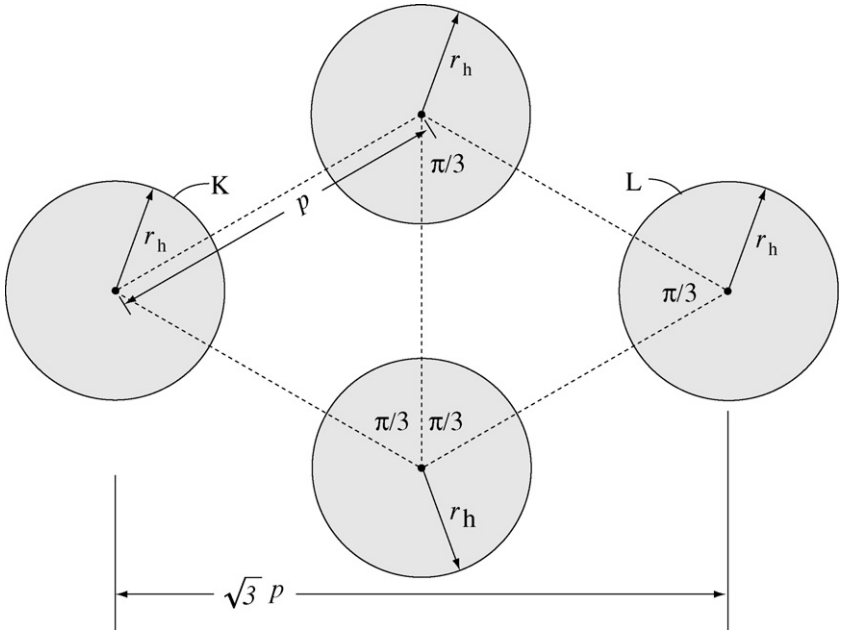

Fig. 8. Geometric layout for the configuration factor between two hexagonal cylinders, partially blocked by two off-axis hexagonal cylinders.

Fig. 2, this configuration factor applies for 3a to 3b, 3a to 6b, etc.

$$F_{KL} = \frac{2}{3} + \frac{1}{2\pi r_h}\left[-p\sqrt{1-\frac{4r_h^2}{p^2}} + \sqrt{3p^2-(2r_h)^2}\right] - \frac{1}{2\pi r_h}\left[p\sqrt{1-\frac{(2r_h)^2}{p^2}}\right] + \frac{1}{\pi}\left[\cos^{-1}\left(\frac{2r_h}{p}\right) + \cos^{-1}\left(\frac{2r_h}{p}\right) + \sin^{-1}\left(\frac{2r_h}{\sqrt{3}p}\right)\right] \quad (7)$$

The restriction on this configuration factor is

$$\frac{1}{4} \le \frac{r_h}{p} \le \frac{1}{2} \quad (8)$$

The lower bound assures that the cylinders do not overlap. The upper bound assures that the off-axis cylinders block some radiation. If the off-axis cylinders do not block radiation, then Eq. (2) is appropriate, using the separation distance as $\sqrt{3}p$ instead of p.

2.7. Hexagonal cylinder to hexagonal cylinder, blocked by an off-axis center cylinder and an off-axis hexagonal cylinder

Fig. 9 illustrates the layout for the configuration factor from a hexagonal cylinder (r_h) to another hexagonal cylinder (r_h) that is partially blocked by a center (r_c) and a hexagonal (r_h) off-axis cylinder. The centers of all cylinders are at the apexes of equilateral triangles with sides of length p. For example in Fig. 2, this

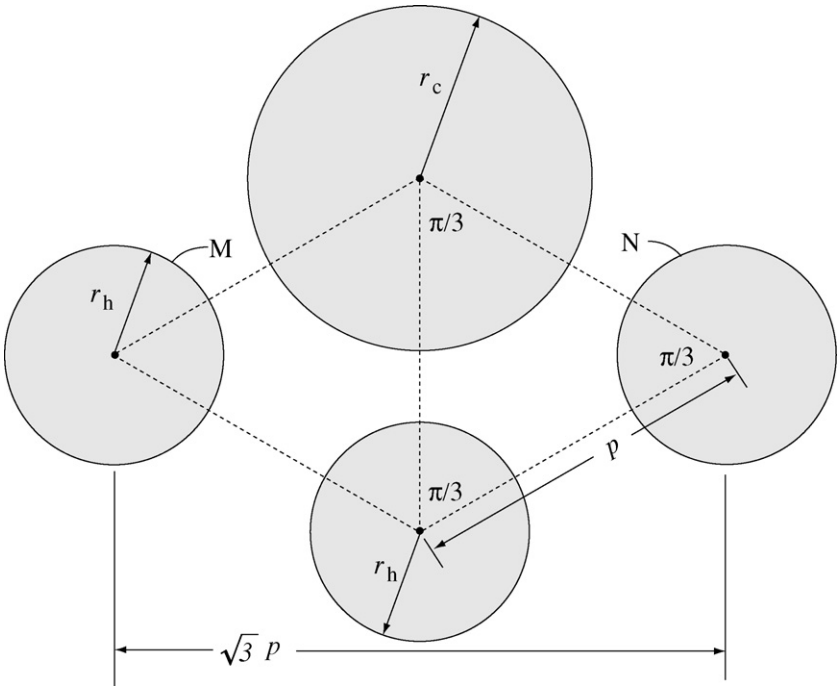

Fig. 9. Geometric layout for the configuration factor between two hexagonal cylinders, partially blocked by off-axis center and hexagonal cylinders.

configuration factor applies for 2a to 2c, 2a to 2e, etc.

$$F_{MN} = \frac{1}{12\pi r_h}[-\pi r_c - 3\pi r_h] + \frac{1}{4\pi r_h}\left[2p\sqrt{1-\frac{(r_c-r_h)^2}{p^2}} - p\sqrt{1-\frac{4r_h^2}{p^2}}\right] - \frac{1}{4\pi r_h}\left[p\sqrt{1-\frac{(r_c+r_h)^2}{p^2}}\right] + \frac{1}{2\pi r_h}\left[2r_h\cos^{-1}\left(\frac{2r_h}{p}\right)\right] + \frac{1}{2\pi r_h}\left[(r_c-r_h)\sin^{-1}\left(\frac{r_c-r_h}{p}\right)\right] \quad (9)$$

Eq. (9) is restricted by

$$\frac{1}{2} \le \frac{r_c+r_h}{p} \le 1 \quad (10)$$

$$\frac{1}{4} \le \frac{r_h}{p} \le \frac{1}{2} \quad (11)$$

The lower bounds assure that the cylinders do not overlap. The upper bounds assure that there is at least some obstruction by both off-axis cylinders.

2.8. Hexagonal cylinder to hexagonal cylinder, blocked by two staggered hexagonal off-axis cylinders

Fig. 10 illustrates the layout for the configuration factor from a hexagonal cylinder (r_h) to another hexagonal cylinder (r_h) that is partially blocked by two staggered off-axis hexagonal cylinders (r_h). The centers of all cylinders are at the apexes of equilateral triangles with sides of length p. For example in Fig. 2, this configuration factor applies for 2a to 6b, 5a to 5c, etc.

$$F_{OP} = \frac{1}{4\pi r_h}\left[p\sqrt{1-\frac{4r_h^2}{p^2}} - 2p\sqrt{3-\frac{4r_h^2}{p^2}} + p\sqrt{7-\frac{4r_h^2}{p^2}}\right] + \frac{1}{2\pi r_h}\left[r_h\sin^{-1}\left(\frac{2r_h}{p}\right) - 2r_h\sin^{-1}\left(\frac{2r_h}{\sqrt{3}p}\right)\right] + \frac{1}{2\pi r_h}\left[r_h\sin^{-1}\left(\frac{2r_h}{\sqrt{7}p}\right) - r_h\tan^{-1}\left(\frac{\sqrt{3}}{5}\right)\right] \quad (12)$$

Eq. (12) is restricted by

$$\frac{2r_h}{p} \le 1 \quad (13)$$

$$\frac{\pi}{3} + \sin^{-1}\left(\frac{2r_h}{\sqrt{3}p}\right) - \cos^{-1}\left(\frac{2r_h}{p}\right) > 0 \quad (14)$$

The first restriction assures that the cylinders do not overlap. The second restriction assures that there is at least some obstruction by both off-axis cylinders.

2.9. Hexagonal cylinder to hexagonal cylinder, blocked by a center and two staggered hexagonal off-axis cylinders

Fig. 11 illustrates the layout for the configuration factor from a hexagonal cylinder (r_h) to another hexagonal cylinder (r_h) that is partially blocked by an off-axis center cylinder (r_c) and two off-axis hexagonal cylinders (r_h). The centers of all cylinders are at the apexes of equilateral triangles with sides of length p. For example in Fig. 2, this configuration factor applies for 2a to 4c, 2a to 4e, etc.

$$F_{QR} = \frac{1}{24\pi r_h}\left[-\pi r_c - 12r_h\tan^{-1}\left(\frac{\sqrt{3}}{5}\right)\right] + \frac{1}{4\pi r_h}\left[+p\sqrt{1-\frac{4r_h^2}{p^2}} - p\sqrt{3-\frac{4r_h^2}{p^2}} + p\sqrt{7-\frac{4r_h^2}{p^2}}\right] + \frac{1}{4\pi r_h}\left[-p\sqrt{1-\frac{(r_c+r_h)^2}{p^2}} - p\sqrt{1-\frac{(r_c-r_h)^2}{p^2}}\right] + \frac{1}{4\pi r_h}\left[-r_c\sin^{-1}\left(\frac{r_c-r_h}{p}\right) + r_c\cos^{-1}\left(\frac{r_c+r_h}{p}\right)\right]$$

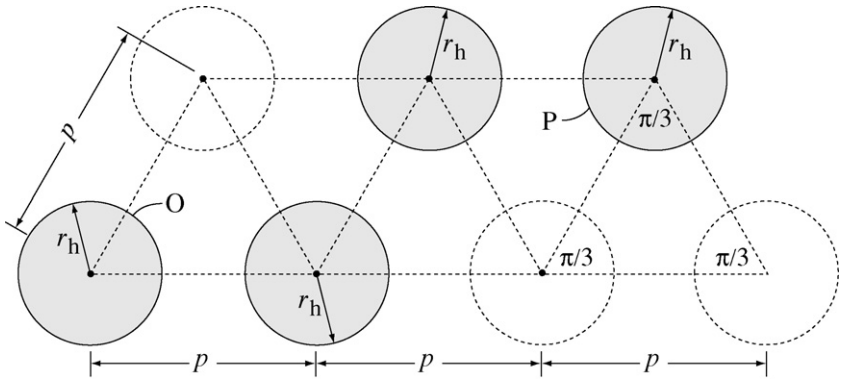

Fig. 10. Geometric layout for the configuration factor between two staggered hexagonal cylinders, partially obstructed by two staggered off-axis hexagonal cylinders.

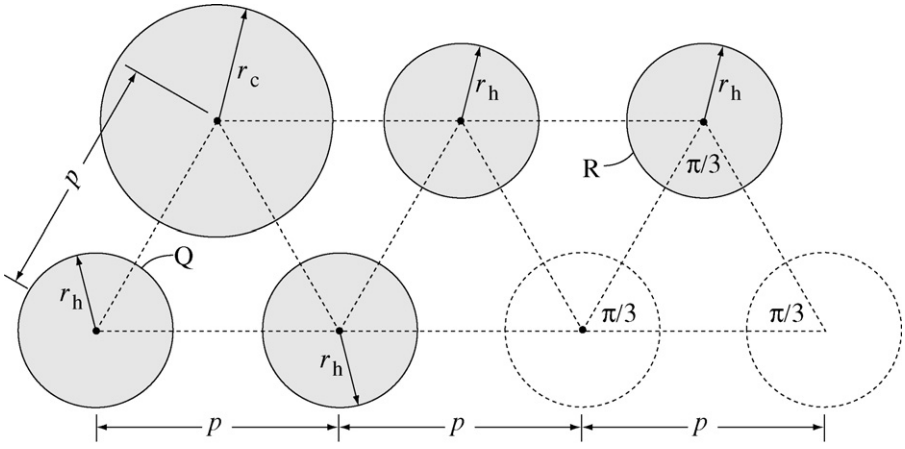

Fig. 11. Geometric layout for the configuration factor between two hexagonal cylinders, partially blocked by a center and two staggered hexagonal off-axis cylinders.

$$+\frac{1}{2\pi r_h}\left[r_h \sin^{-1}\left(\frac{2r_h}{p}\right) - 2r_h \sin^{-1}\left(\frac{2r_h}{\sqrt{3}p}\right)\right]$$

$$+\frac{1}{2\pi r_h}\left[r_h \sin^{-1}\left(\frac{2r_h}{\sqrt{7}p}\right)\right] \quad (15)$$

Eq. (15) is restricted by

$$\frac{2r_h}{p} \le 1 \quad (16)$$

$$\frac{r_c + r_h}{p} \le 1 \quad (17)$$

$$\frac{\pi}{3} + \sin^{-1}\left(\frac{2r_h}{\sqrt{3}p}\right) - \cos^{-1}\left(\frac{2r_h}{p}\right) > 0 \quad (18)$$

$$\frac{\pi}{6} + \sin^{-1}\left(\frac{r_c + r_h}{p}\right) - \cos^{-1}\left(\frac{r_c + r_h}{p}\right) > 0 \quad (19)$$

The first two restrictions assure that the cylinders do not overlap. The second two restrictions assure that there is at least some blockage by each of the off-axis cylinders. If the off-axis cylinders do not block then the configuration factor can be evaluated from Eq. (2), but with the separation distance being $\sqrt{7}p$, not p.

2.10. Center cylinder to hexagonal cylinder, blocked by three staggered off-axis hexagonal cylinders

Fig. 12 illustrates the layout for the configuration factor from a center cylinder (r_c) to a hexagonal cylinder (r_h) that is partially blocked by three staggered off-axis hexagonal cylinders (r_h). The centers of all cylinders are at the apexes of equilateral triangles with sides of length p. For example in Fig. 2, this configuration factor applies for 1 to 5c, 1 to 5d, etc.

$$F_{ST} = \frac{1}{24\pi r_c}\left[\pi(r_c - 4r_h) + 6p\left(\sqrt{1 - \frac{4r_h^2}{p^2}} - \sqrt{3 - \frac{4r_h^2}{p^2}}\right)\right]$$
$$+\frac{1}{4\pi r_c}\left[\sqrt{7p^2 - (r_c + r_h)^2} - \sqrt{3p^2 - (r_c + r_h)^2}\right]$$
$$+\frac{r_h}{4\pi r_c}\left[\cos^{-1}\left(\frac{2r_h}{p}\right) + 3\sin^{-1}\left(\frac{2r_h}{p}\right)\right]$$
$$-\frac{r_h}{4\pi r_c}\left[2\sin^{-1}\left(\frac{2r_h}{\sqrt{3}p}\right)\right]$$
$$-\frac{(r_c + r_h)}{4\pi r_c}\left[\sin^{-1}\left(\frac{r_c + r_h}{\sqrt{3}p}\right) - \sin^{-1}\left(\frac{r_c + r_h}{\sqrt{7}p}\right)\right]$$
$$-\frac{(r_c + r_h)}{4\pi r_c}\left[\tan^{-1}\left(\frac{\sqrt{3}}{5}\right)\right] \quad (20)$$

Eq. (20) is restricted by

$$\frac{2r_h}{p} \le 1 \quad (21)$$

$$\frac{r_c + r_h}{p} \le 1 \quad (22)$$

$$\frac{\pi}{3} + \sin^{-1}\left(\frac{r_c + r_h}{\sqrt{3}p}\right) - \cos^{-1}\left(\frac{2r_h}{p}\right) > 0 \quad (23)$$

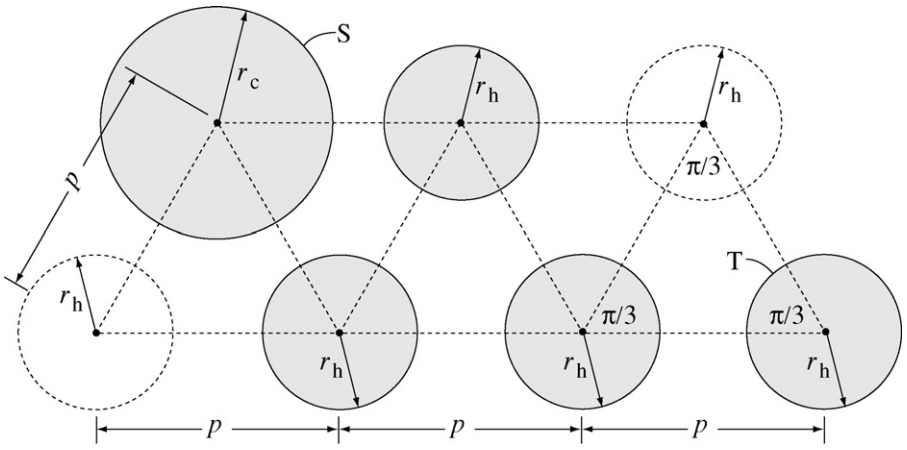

Fig. 12. Geometric layout for the configuration factor between a center cylinder and a hexagonal cylinder, partially blocked by three staggered off-axis hexagonal cylinders.

$$\frac{\pi}{3} + \sin^{-1}\left(\frac{2r_h}{p}\right) - \cos^{-1}\left(\frac{r_c + r_h}{\sqrt{3}p}\right) > 0 \tag{24}$$

The first two restrictions assure that the cylinders do not overlap. The second two restrictions assure that there is at least some blockage by each of the off-axis cylinders.

3. Configuration-factor matrix

Solving the radiation balance requires evaluation of an entire configuration-factor matrix. The configuration factor F_{ij} represents the fraction of radiation leaving surface i that impinges upon surface j. Although there are 36 cylinders in this example, the symmetry denoted by the numbering in Fig. 2 shows that there are only 7 effective surfaces. That is, all similarly numbered surfaces behave exactly alike. Thus the configuration-factor matrix is a 7×7 matrix. A further assumption in the analysis that follows is that all similarly numbered surfaces have the same temperature. Because the configuration factors derived here apply only to two dimensional surfaces (i.e., long cylinders), the analysis does not permit axial variation along the length of the cylinders.

The configuration factor from the center cylinder to one of the cylinders numbered 2 (e.g., $F_{1,2a}$) is evaluated using Eq. (1) as F_{AB}. Because there are 6 tubes of type 2, the net configuration factor from 1 to 2 is $F_{12} = 6F_{AB}$. It follows directly from configuration-factor reciprocity that $F_{21} = A_1F_{12}/A_2$, where $A_1 = 2\pi r_c$ and $A_2 = 6 \times (2\pi r_h)$ are the total areas per unit length of cylinders. Following an analogous approach

$$F_{13} = 6F_{IJ}, \qquad F_{14} = 6F_{EF}, \qquad F_{15} = 12F_{ST}, \qquad F_{16} = 6F_{GH} \tag{25}$$

$$F_{31} = \frac{A_1F_{13}}{A_3}, \qquad F_{41} = \frac{A_1F_{14}}{A_4}, \qquad F_{51} = \frac{A_1F_{15}}{A_6}, \qquad F_{61} = \frac{A_1F_{16}}{A_6} \tag{26}$$

The configuration factor from the surface of the center cylinder to itself is zero. In this example, it may be seen that several cylinders are completely obscured from other cylinders. Specifically,

$$F_{11} = 0, \qquad F_{44} = 0, \qquad F_{66} = 0 \tag{27}$$

The cylinders labeled 2 can partially see each other. For example, some radiation from cylinder 2a can reach cylinder 2b, 2c, 2e, and 2f. Using well-known configuration-algebra rules for composite surfaces

$$\begin{aligned} A_2F_{22} &= A_{(2a-2f)}F_{(2a-2f),(2a-2f)} \\ &= A_{2a}F_{2a,(2a-2f)} + A_{2b}F_{2b,(2a-2f)} + \cdots + A_{2f}F_{2f,(2a-2f)} \end{aligned} \tag{28}$$

where $A_2 = A_{(2a-2f)}$ is the total surface area of all cylinders labeled 2. The configuration factor from each of the cylinders labeled 2 to the four other cylinders 2 that it can see can be represented as, for example,

$$F_{2a,(2a-2f)} = F_{2a,2b} + F_{2a,2f} + F_{2a,2c} + F_{2a,2e} = 2F_{CD} + 2F_{MN} \tag{29}$$

Because all the cylinders have the same surface area and each of the cylinders 2 see neighboring cylinders 2 in geometrically the same way, it follows that

$$F_{22} = 2F_{CD} + 2F_{MN} \tag{30}$$

Following analogous analysis, it can be shown that

$$F_{33} = 2F_{KL}, \qquad F_{55} = F_{AB} + 2F_{KL} + 2F_{OP} \tag{31}$$

The configuration factors from cylinders 2 to the other hexagonal cylinders can be evaluated as

$$F_{23} = 2F_{CD}, \qquad F_{24} = F_{CD} + 2F_{KL} + 2F_{QR} \tag{32}$$

$$F_{25} = 2F_{KL} + 2F_{OP}, \qquad F_{26} = 2F_{OP} \tag{33}$$

The configuration factors from cylinders 3 to the other hexagonal cylinders can be evaluated as

$$F_{34} = 2F_{CD} + 2F_{OP}, \qquad F_{35} = 2F_{CD} + 2F_{OP} \tag{34}$$

$$F_{36} = 2F_{KL} \tag{35}$$

The configuration factors from cylinders 4 to the other hexagonal cylinders can be evaluated as

$$F_{45} = 2F_{CD} + 2F_{KL}, \qquad F_{46} = F_{CD} + 2F_{OP} \tag{36}$$

The configuration factors from cylinders 5 to cylinders 6 can be evaluated as

$$F_{56} = F_{CD} \tag{37}$$

All other configuration factors to complete the matrix can be evaluated from reciprocity

$$F_{ji} = \frac{A_iF_{ij}}{A_j} \tag{38}$$

and row-summation

$$\sum_{j=1}^{N} F_{ij} = 1 \tag{39}$$

where N is the number of surfaces on the cavity. In the present example $N = 7$. The areas needed for reciprocity are evaluated using the total surface area for all the cylinders of a certain number. That is, for example,

$$A_5 = A_{(5a,5b,\ldots,5l)} = 12 \times (2\pi r_h). \tag{40}$$

4. Thermal energy balance

The fuel-cell tubes produce heat, which must be transferred by a combination of radiation and convection to the surroundings. To illustrate the primary features of the heat transfer, the convection is modeled in terms of a heat-transfer coefficient h that is assumed to be spatially uniform. Temperature of the air flowing outside the tube is also assumed to be spatially uniform. This uniform stirred-reactor model satisfies the overall heat balance and is sufficient to show the overall trends in the convective and radiation heat transfer. The air temperature T_a is determined from an energy balance that depends upon the inlet air temperature $T_{a,in}$, the mass flow rate $\dot{m}$, the tube surface temperatures T_i.

Assume an example in which the hexagonal cylinders are SOFC tubes with a typical electrical power density of $Q_e = 0.30\,W\,cm^{-2}$ and a conversion efficiency of $\eta = 45\%$. The thermal heat flux through the tube surfaces Q_t is determined from

$$\eta = \frac{Q_e}{Q_e + Q_t} \tag{41}$$

The specific surface area (i.e., area per unit length) of an individual tube is $A_h = 2\pi r_h = 3.14 \times 10^{-2}\,m^2/m$. Under these circumstances the thermal flux (per unit length) is $Q_t = 115.2\,W/m$. For the example, assume that the outer shell (surface 7) is held at a fixed temperature of $T_7 = 600\,^\circ C$ (873 K) and that the center cylinder (surface 1) is a perfect thermal insulator, specified as $Q_{net,1} = 0$.

The thermal radiation leaving the tube surfaces is the difference between the heat dissipated by the fuel cell and the convection from the tube surface to the surrounding air. That is,

$$Q_{rad,i} = n_i Q_t - hA_i(T_i - T_a) \tag{42}$$

where n_i is the number of type-i tubes. Assuming grey diffuse surfaces, the thermal radiation entering a cavity from each surface can be represented alternatively as

$$Q_{rad,i} = A_i \epsilon_i \frac{\sigma T_i^4 - J_i}{1 - \epsilon_i} \tag{43}$$

and

$$Q_{rad,i} = \sum_{j=1}^{N} A_i F_{ij}(J_i - J_j) \tag{44}$$

where A_i, J_i, and ϵ_i are the specific surface area, the radiosity, and emissivity surface of surface i.

Energy balances for each surface as functions of the temperatures T_i and radiosities J_i may be written as

$$Q_{rad,1} = Q_{net,1} - hA_1(T_1 - T_a) = \sum_{j=1}^{7} A_1 F_{1j}(J_1 - J_j) \tag{45}$$

$$Q_{rad,2} = 6Q_t - hA_2(T_2 - T_a) = \sum_{j=1}^{7} A_2 F_{2j}(J_2 - J_j) \tag{46}$$

$$Q_{rad,3} = 6Q_t - hA_3(T_3 - T_a) = \sum_{j=1}^{7} A_3 F_{3j}(J_3 - J_j) \tag{47}$$

$$Q_{rad,4} = 6Q_t - hA_4(T_4 - T_a) = \sum_{j=1}^{7} A_4 F_{4j}(J_4 - J_j) \tag{48}$$

$$Q_{rad,5} = 12Q_t - hA_5(T_5 - T_a) = \sum_{j=1}^{7} A_5 F_{5j}(J_5 - J_j) \tag{49}$$

$$Q_{rad,6} = 6Q_t - hA_6(T_6 - T_a) = \sum_{j=1}^{7} A_6 F_{6j}(J_6 - J_j) \tag{50}$$

$$Q_{rad,7} = A_7 \epsilon_7 \frac{\sigma T_7^4 - J_7}{1 - \epsilon_7} = \sum_{j=1}^{7} A_7 F_{7j}(J_7 - J_j) \tag{51}$$

$$Q_{rad,1} = Q_{net,1} - hA_1 * (T_1 - T_a) = A_1 \epsilon_1 \frac{\sigma T_1^4 - J_1}{1 - \epsilon_1} \tag{52}$$

$$Q_{rad,2} = 6Q_t - hA_2(T_2 - T_a) = A_2 \epsilon_2 \frac{\sigma T_2^4 - J_2}{1 - \epsilon_2} \tag{53}$$

$$Q_{rad,3} = 6Q_t - hA_3(T_3 - T_a) = A_3 \epsilon_3 \frac{\sigma T_3^4 - J_3}{1 - \epsilon_3} \tag{54}$$

$$Q_{rad,4} = 6Q_t - hA_4(T_4 - T_a) = A_4 \epsilon_4 \frac{\sigma T_4^4 - J_4}{1 - \epsilon_4} \tag{55}$$

$$Q_{rad,5} = 12Q_t - hA_5(T_5 - T_a) = A_5 \epsilon_5 \frac{\sigma T_5^4 - J_5}{1 - \epsilon_5} \tag{56}$$

$$Q_{rad,6} = 6Q_t - hA_6(T_6 - T_a) = A_6 \epsilon_6 \frac{\sigma T_6^4 - J_6}{1 - \epsilon_6} \tag{57}$$

$$\dot{m} c_p (T_a - T_{a,in}) = \sum_{i=1}^{7} hA_i(T_i - T_a) \tag{58}$$

Assuming that the air surrounding the tubes is perfectly mixed and spatially uniform, Eq. (58) is an energy balance for the flowing air. This significantly simplifying assumption means that inlet air mixes instantly with air already within the volume surrounding the tubes, and that the air temperature leaving the volume is the same as the mixture temperature. The perfectly-stirred-reactor assumption is usually justified at flow rates with high turbulent mixing. Although the perfect-mixing assumption could be questioned, especially at low air flow rates, the approximation is appropriate to evaluate the relative effects of convection and radiation.

The air mass flow rate can be represented in terms of the oxygen flow needed to support fuel oxidation. Assuming a current density i ($A\,m^{-2}$), the stoichiometric molar flow rate of air per unit length is

$$\dot{N}_{air,stoich} = \frac{1}{0.21}\frac{i}{4F} \tag{59}$$

where F is the Faraday constant. The stoichiometric air mass flow rate (i.e., mass flow rate per unit tube length, $kg\,s^{-1}\,m^{-1}$) needed to support all the tubes in the stack is

$$\dot{m}_{air,stoich} = \dot{N}_{air,stoich} W_{air} A_{tube} n_{tubes}, \tag{60}$$

where W_{air} is the molecular weight of air, $A_{tube} = 2\pi r_h$ is the specific area (area per unit length) of a single SOFC tube, and n_{tubes} is the number of tubes in the stack. In practice, fuel-cell stacks are operated with significantly more than the stoichiometric air flow. Thus, the net air flow is

$$\dot{m} = S\dot{m}_{air,stoich}, \tag{61}$$

where S is the number of "stoichs" (i.e., the factor by which the actual air flow exceeds the stoichiometric air flow). For a current density of $i = 0.4\,A\,cm^{-2}$ and $S = 4$, with 36 tubes the net air mass flow rate is $\dot{m} = 6.47 \times 10^{-3}\,kg\,s^{-1}\,m^{-1}$.

Eqs. (45)–(58) form a system of 14 nonlinear equations for the radiosities J_1 on each of 7 surfaces, the temperatures on T_i on surfaces 1 through 6 (the outer shell temperature T_7 is specified), and the air temperature T_a.

Table 1
Nominal stack and operating parameters.

Parameters	Value	Units
Stack geometry		
SOFC tube radius (r_h)	5	mm
Center-post radius (r_h)	7.5	mm
Outer shell radius (r_o)	61.25	mm
Tube spacing pitch (p)	17.5	mm
Stack operating conditions		
Cell power density (P)	0.3	W cm^{-2}
Conversion efficiency (η)	0.45	
Cell current density (i)	0.4	A cm^{-2}
"Stoichs" of air flow (S)	4	
Air flow rate ($\dot{m}$)	0.00647	kg s^{-1} m^{-1}
Inlet air temperature ($T_{in,air}$)	500	°C
Outer shell temperature (T_7)	600	°C
Heat production per cell (Q_i)	115.2	W m^{-1}
Center-post heat transfer (Q_1)	0	W m^{-1}
Radiation parameters		
Center-post emissivity (ϵ_1)	0.8	
Outer shell emissivity (ϵ_7)	0.8	
SOFC tube emissivity ($\epsilon_2 - \epsilon_6$)	0.6	
Convection parameters		
Heat transfer coefficient	20	W m^{-2} K^{-1}

Table 2
Individual configuration factors with $p = 17.5$ mm, $r_c = 7.5$ mm, and $r_h = 5$ mm.

Configuration factor	Value
F_{AB}	9.578×10^{-2}
F_{CD}	9.371×10^{-2}
F_{EF}	1.900×10^{-3}
F_{GH}	6.321×10^{-4}
F_{IJ}	4.396×10^{-2}
F_{KL}	4.966×10^{-2}
F_{MN}	7.063×10^{-2}
F_{OP}	8.627×10^{-3}
F_{QR}	6.362×10^{-3}
F_{ST}	7.216×10^{-3}

5. Computational implementation

The intent of the model is to provide a tool that can be used to quickly evaluate potential design and operational tradeoffs. The model is easily programmed, such as in a spread sheet environment. Beyond evaluating explicit functions (e.g., the configuration factor matrix), the computational implementation must be capable of solving a system of nonlinear equations (i.e., Eqs. (45)–(58)).

6. Example and parameter studies

Table 1 lists geometric parameters and operating conditions for a nominal system. The model is used to evaluate the influence of certain parameters.

6.1. Configuration factor evaluation

Consider a specific bundle with $p = 17.5$ mm, $r_c = 7.5$ mm, and $r_h = 5$ mm. Table 2 lists the individual configuration factors. Table 3 lists a full configuration matrix F_{ij}, evaluated for the example geometric parameters.

6.2. Effect of heat-transfer coefficient

Figs. 13 and 14 illustrate the effects of varying heat-transfer coefficient on the tube temperatures and the convective heat transfer. In this study, the emissivity of the SOFC tubes (i.e., A_2–A_6) is $\epsilon = 0.6$, while the emissivity of the center post (A_1) and outer shell (A_7) is $\epsilon = 0.8$. The center post is assumed to be perfectly insulated and the outer shell is fixed at $T_7 = 600$ °C. The net air mass flow rate is $\dot{m} = 6.47 \times 10^{-3}$ kg s^{-1} m^{-1} (a factor of 4 times the stoichiometrically required air) and the inlet-air temperature is $T_{a,in} = 500$ °C. When $h = 0$, the heat transfer from the SOFC tubes to the outer shell is via thermal radiation alone.

Even though the overall air flow is four times that required to supply oxygen to the fuel cells, the Reynolds numbers and convective heat transfer coefficients for the geometry and operating conditions of Table 1 are low; Reynolds numbers are under 100, and the heat-transfer coefficients are in the range $3 < h < 10$ W m^{-2} K^{-1}. In these ranges, the primary mode of heat transfer

Table 3
Configuration factor matrix with $p = 17.5$ mm, $r_c = 7.5$ mm, and $r_h = 5$ mm.

	1	2	3	4	5	6	7
1	0.0000	0.5747	0.2638	0.0114	0.0866	0.0038	0.0598
2	0.1437	0.3287	0.1875	0.1944	0.1166	0.0173	0.0121
3	0.0659	0.1874	0.0993	0.2047	0.2047	0.0993	0.1387
4	0.0028	0.1943	0.2047	0.000	0.2867	0.1110	0.2004
5	0.0108	0.0583	0.1023	0.1434	0.1606	0.0937	0.4309
6	0.0009	0.0173	0.0993	0.1110	0.1874	0.000	0.5841
7	0.0073	0.0059	0.0679	0.0982	0.4221	0.2861	0.1125

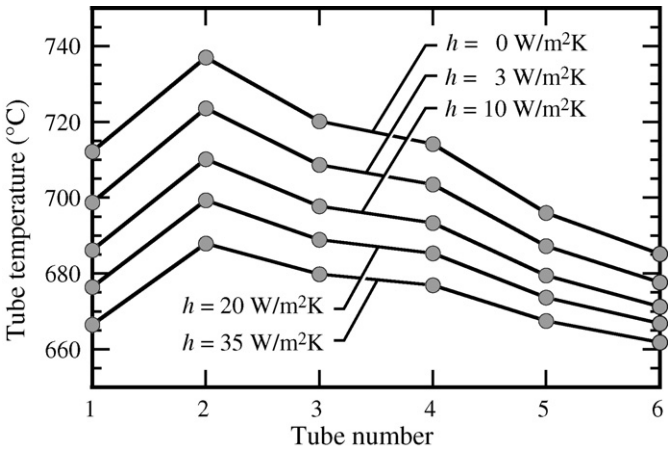

Fig. 13. The effect of heat transfer coefficient on the tube temperatures.

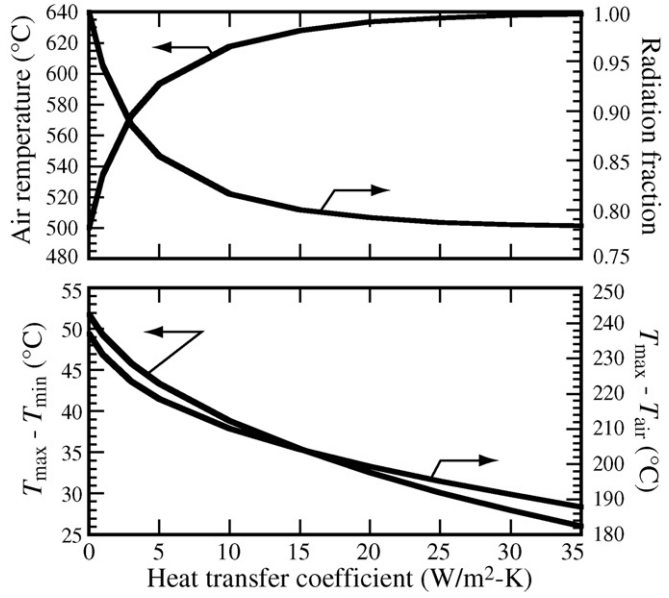

Fig. 14. The effect of heat transfer coefficient on stack temperatures and heat-transfer characteristics.

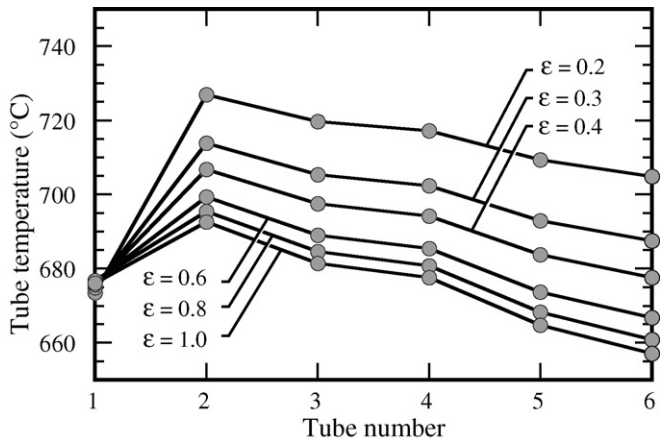

Fig. 15. The effect of emissivity on tube temperatures.

from the tubes to the ultimate heat sink is via radiation to the outside wall. Fig. 14 shows the ratio of the radiation heat transfer to the total heat removed from the tubes. For a heat-transfer coefficient $h = 10\,\mathrm{W\,m^{-2}\,K^{-1}}$, 82% of the heat transfer is by radiation and 18% by convection.

6.3. Effect of SOFC emissivity

Fig. 15 shows the effect of emissivity on the surfaces of the SOFC tubes. In all cases, the emissivity of the center post and outer shell is $\epsilon = 0.8$. The center post is assumed to be perfectly insulated and the outer shell is fixed at $T_7 = 600\,^{\circ}\mathrm{C}$. The net air mass flow rate is $\dot{m} = 6.47 \times 10^{-3}\,\mathrm{kg\,s^{-1}\,m^{-1}}$ and the inlet-air temperature is $T_{\mathrm{a,in}} = 500\,^{\circ}\mathrm{C}$. The heat-transfer coefficient is fixed at $h = 20\,\mathrm{W\,m^{-2}\,K^{-1}}$. The outer fuel-cell tubes behave as radiation shields, impeding radiative transport to the outer shell. Lower emissivity (i.e., high reflectivity) produces higher tube temperatures.

Fig. 16 further summarizes the effects of SOFC tube emissivity. The maximum SOFC temperature (i.e., T_2) is always much higher than the outer-shell temperature (T_7). As emissivity increases

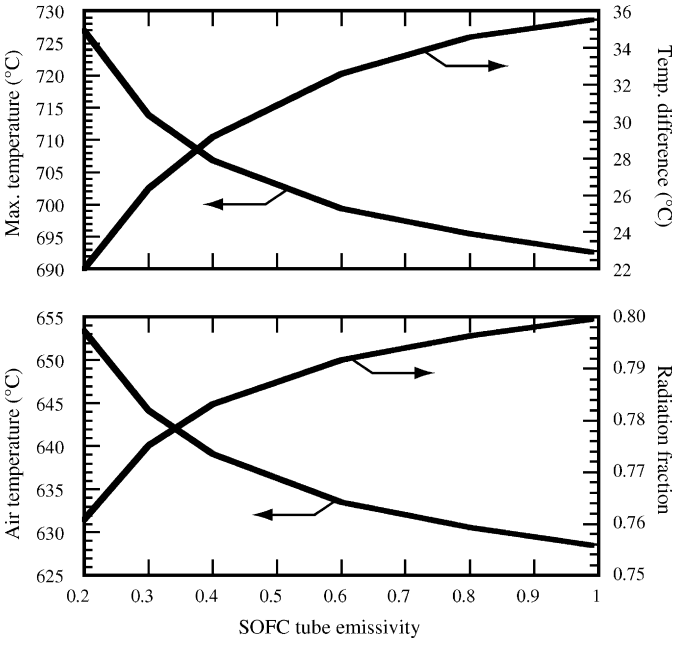

Fig. 16. The effect of SOFC tube emissivity on stack temperatures and heat-transfer characteristics.

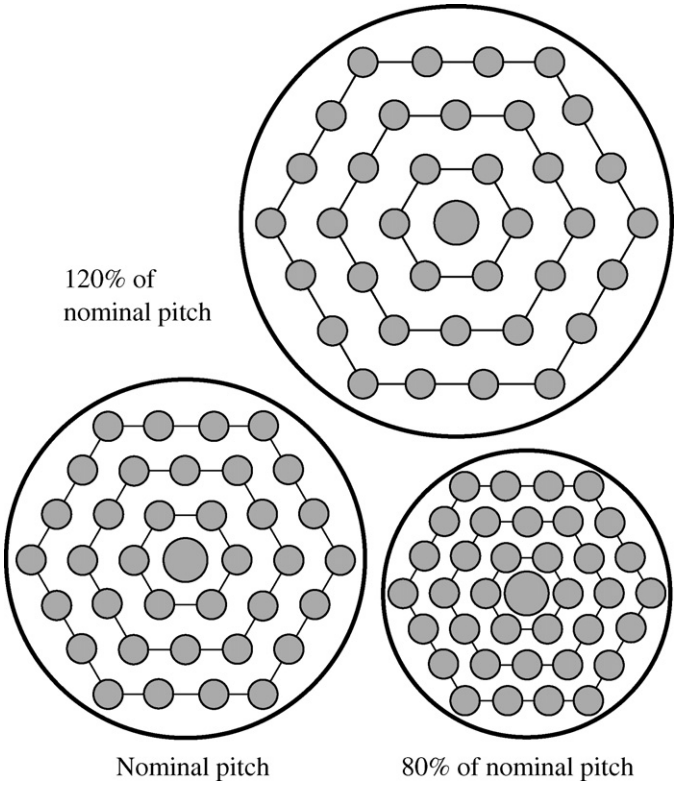

Fig. 17. Scaled layouts of the nominal bundle layout and bundles for which the nominal pitch ($p = 17.5$ mm) is scaled by 80% and 120%. SOFC tube and center-post radii are the same in all cases.

from $\epsilon = 0.2$ to $\epsilon = 0.99$, the maximum temperature decreases by approximately 30 °C. The temperature difference between the hottest SOFC tubes (T_2) and the coolest SOFC tubes (T_6) increases slightly as emissivity increases. Under the circumstances here about 75% of the heat produced by the SOFC tubes is transferred to the outer shell by radiation. In other words, approximately 25% of the heat is carried out with the cathode air. Although a relatively weak effect, higher emissivity causes a higher fraction of the total heat produced by the SOFC tubes to be transferred to the outer shell by radiation. Because high emissivity increases radiative transport, convective transport is diminished. This effect causes the air temperature to decrease from about 655 °C for $\epsilon = 0.2$ to approximately 630 °C for $\epsilon = 0.99$.

6.4. Effect of tube pitch

Fig. 17 illustrates (to scale) the nominal dimensions for a tube layout as well as layouts for which the pitch p is 80% of the nominal (i.e., $p = 14$ mm) and 120% of the nominal (i.e., $p = 21$ mm). The outer shells are also scaled by 80% and 120%. The SOFC tube and center-post radii are the same in all cases. In the compact packing case the radiation from inner SOFC tubes to the outer shell is significantly impeded compared to the expanded case.

Fig. 18 shows the effect of pitch on tube temperatures. All parameters, except pitch and outer shell radius, are the same as those listed in Table 1. The compact pitch (80% case) causes higher temperatures as well as higher temperature differences between tubes. The expanded pitch (120%) yields lower and more uniform tube temperatures. Assuming that temperature uniformity is desirable, the expanded pitch may be beneficial for performance. However, the more uniform tube temperatures came at the expense of lower packing density.

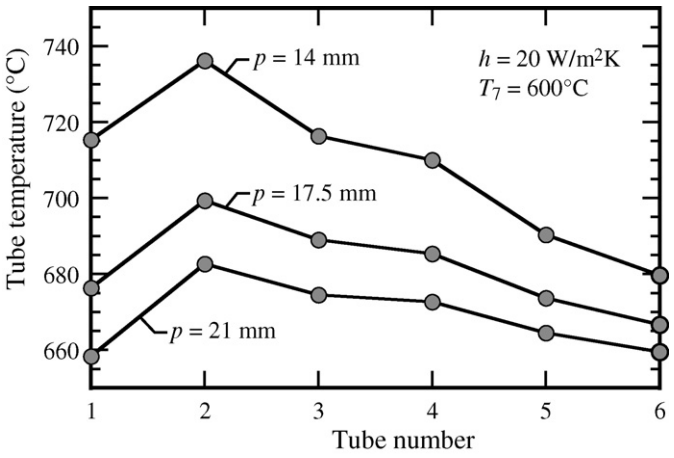

Fig. 18. Effect of pitch on tube temperatures.

7. Summary and conclusions

This model can be used to explore numerous design and operational alternatives. The key outputs of the model are the average cell temperatures and the cell temperature gradients as a function of stack geometry, operating conditions, and the emissivity of surfaces. The model quickly yields information on the total radiation heat transfer and the ratio of radiation to convection within the stack. With this information, stack designers can quickly assess the impact of design alternatives. For example, raising the outer wall temperature (e.g., through the use of better insulation) increases the average cell temperatures while decreasing the temperature differences between cells. Because a majority of the heat transfer from the cells is through radiation, reducing the emissivity of the outer wall is a powerful lever to control the stack temperature.

Radiative heat transfer proves remarkably effective at removing the heat from tube bundles of this size. At typical operating conditions, most tubes operate less than 100 °C hotter than the outer wall, and the maximum temperature difference across the bundle is under 30 °C. Less than 20% of the heat transferred from the tubes under these conditions is by convection to the cathode air (i.e., around 80% is transferred by radiation).

For relatively small tube bundles as considered here, lower air flows can be employed advantageously. This is particularly important for portable applications, where higher air flows can lead to high parasitic power draw in the cathode air supply system. The ability to reject heat directly from the cells by radiation to the outside walls provides the stack designer with additional flexibility in selecting the cathode air flow rate.

In all cases the interior tube temperatures are greater than the fixed outer-shell temperature of 600 °C, with the inner fuel-cell ring (A_2) achieving the highest temperature. The temperature difference between the hottest and coolest SOFC tube is around 30 °C, with the difference increasing slightly with increasing emissivity.

Although there are similarities, there are also significant differences in the thermal behavior of planar and tubular stacks. In both cases, heat is transferred convectively to gas flow (primarily cathode air) and by a combination of modes to the exterior housing of the stack. In planar stacks, heat is transferred to the periphery of the stack by conduction through the interconnect plates and the membrane-electrode assemblies, which can cause significant temperature differences within the stack. By contrast, as shown in the present paper, for stacks consisting of a bundle of tubes, thermal radiation plays a significant role in transferring heat from the tubular cells to the periphery of the stack. Tubular stacks can be designed to take advantage of radiation, yielding additional design freedom to control the relative influences of convective and radiation in heat rejection. In large planar stacks, the majority of the heat produced in the stack must be removed by convection to the cathode air, not by conduction through the solid materials of the stack. This often forces designers to use higher cathode flows than would otherwise be required to maintain cell temperature variations within acceptable limits. Because high cathode-air flow draws significant parasitic power from the system, tubular stacks that can beneficially use radiation to assist thermal management reduce the parasitic losses associated with high cathode air flows.

The present model is simple relative to a full three-dimensional computational simulation. However, it is also mostly analytic and can be solved easily is a few seconds on a personal computer. Thus, the model provides the capability to rapidly screen alternatives prior to detailed design.

Acknowledgments

This effort was supported by the Office of Naval Research via an RTC grant (N00014-05-1-03339). We gratefully acknowledge insightful discussions with Mr. Kyle Kattke and Prof. Rob Braun (Colorado School of Mines) who are developing three-dimensional computational fluid dynamics models of similar tubular stacks.

References

[1] R. Kee, H. Zhu, A. Sukeshini, G. Jackson, Combust. Sci. Technol. 180 (2008) 1207–1244.
[2] R. Kee, A. Colclasure, H. Zhu, in: J. Garche (Ed.), Encyclopedia of Electrochemical Power Sources, Elsevier, Amsterdam, 2009.
[3] R. Siegel, J. Howell, Thermal Radiation Heat Transfer, 4th ed., Taylor and Francis, London, 2002.
[4] M. Modest, Radiative Heat Transfer, 2nd ed., Academic Press, 2003.
[5] N. Juul, ASME J. Heat Transfer 104 (1982) 384–388.
[6] R. Cox, Radiative heat transfer in arrays of parallel cylinders, Ph.D. Thesis, University of Tennessee, Knoxville, 1976.
[7] Wolfram Research, Inc., Mathematica, Version 7.0, Champaign, IL, 2008.